Multiscale method for Heisenberg spin simulations

Thomas Jourdan,[1] Alain Marty,[2] and Frédéric Lançon[1,*]
[1]*Laboratoire de simulation atomistique (L_Sim), SP2M, INAC, CEA, 38054 Grenoble Cedex 9, France*
[2]*Laboratoire nanostructures et magnétisme (NM), SP2M, INAC, CEA, 38054 Grenoble Cedex 9, France*
(Received 14 March 2008; published 17 June 2008)

A multiscale method that couples classical Heisenberg model to micromagnetics in a unified formalism is presented. It is based on a multiresolution adaptive finite difference mesh, which ensures significant reduction of the number of variables and computation time with respect to either atomistic or micromagnetic simulations, together with a precise description of the modeled system where necessary. The hierarchical structure of the mesh is used to compute efficiently the dipolar field by means of a fast multipole method. The underlying atomistic approach is particularly useful to handle magnetic singularities and describe structural defects. The method is applied here to the case of a magnetic vortex and a thin layer of FePt with a microtwin. Results are compared to fully atomistic and micromagnetic simulations when possible.

DOI: 10.1103/PhysRevB.77.224428 PACS number(s): 75.40.Mg, 75.10.Hk, 75.70.Ak, 75.75.+a

I. INTRODUCTION

Modeling a magnetic system may require to describe precisely a particular area, either because the atomic structure should be taken into account,[1,2] or because the magnetic configuration exhibits steep variations. In this case micromagnetic models[3] fail to give a satisfying description and atomistic models must be considered, which induces a much higher amount of computational effort if the modeled system is large. Indeed to correctly handle the long-ranged dipolar effects, some parts of the system that are uniformly magnetized have to be included in the simulation.

Multiscale modeling provides an elegant way to reduce the computational cost associated with a fully atomistic simulation by describing the system with a high resolution only where it is necessary. In the case of magnetic simulations, modeling at atomic scale may be achieved using classical Heisenberg model. The magnetic energy within such a model can be written as a sum of on-site terms and pair interactions:

$$E = \sum_{s=1}^{n_a} \sum_{t=1}^{s} E_{st}, \tag{1}$$

where n_a is the number of atomic spins. The basic idea of a multiscale method consists of reducing the number of variables by gathering spins, thus writing:

$$E \approx \sum_{s=1}^{n} \sum_{t=1}^{s} E_{st} + \sum_{S=1}^{N} \sum_{t=1}^{n} E_{St} + \sum_{S=1}^{N} \sum_{T=1}^{S} E_{ST}. \tag{2}$$

The notations are the following: n is the number of atomic spins in the multiscale approach, N is the number of macrospins (micromagnetic nodes), such that $N+n \ll n_a$. In the rest of the paper, lowercase indexes s and t refer to atomic quantities and uppercase indexes S and T to macrospins. Greek letters σ and τ are used to refer to atomic sites or macrospins, which are called "nodes" regardless of their type.

Up to now only a few works have been devoted to multiscale simulations in magnetism. Some of them use a multiresolution scheme within a micromagnetic approach, either with finite difference method (FDM)[4] or finite element method (FEM).[5] Methods that couple micromagnetics to the Heisenberg model have been used to describe systems with grain boundaries[1] or an interface between two materials.[6] Modeling of dynamics and the influence of temperature have also been addressed mainly for simple systems.[7–9]

We propose here an approach that seamlessly couples micromagnetics to the Heisenberg model within a single multiscale formalism. An adaptive finite difference method is used to approximate the micromagnetic part of the system. It has been preferred to finite element method, because the constrained remeshing in this latter method, often performed by Delaunay triangulation,[10,11] adds extra complexity and may require significant computation time. Furthermore, the hierarchical structure and geometrical regularity of a finite difference grid can be used to compute the dipolar field with a fast summation scheme, regardless of the nature of the nodes (micromagnetic or atomic). In the following we will focus on equilibrium states. Dynamics and thermal effects will not be included in the simulations.

We first describe the formalism for the different energy terms (Secs. II and III). Numerical considerations on the approximations and the remeshing are addressed in Sec. IV. The multiscale method is used in two model cases, a thin square element containing a vortex and a layer of FePt with a structural defect (Sec. V).

II. EXCHANGE AND ANISOTROPY TERMS

A. Exchange energy

Within the Heisenberg model, the exchange energy between two atomic spins s and t reads:

$$E_{st}^{\mathrm{ex}} = -J_{st}\boldsymbol{m}_s \cdot \boldsymbol{m}_t = -J_{st}m_s m_t \boldsymbol{\alpha}_s \cdot \boldsymbol{\alpha}_t, \tag{3}$$

where $\boldsymbol{\alpha}_s$ and $\boldsymbol{\alpha}_t$ are unit vectors along $\boldsymbol{m}_s$ and $\boldsymbol{m}_t$.

Assuming a low spatial variation of the magnetization, it is possible to derive an expression of the associated density in a continuous approach. A normalized vector field $\boldsymbol{\alpha}(\boldsymbol{r})$ is used to replace the atomic variables $\boldsymbol{\alpha}_s$. In the case of a ferromagnet or locally collinear (rigid) antiferromagnet, we obtain (see Appendix A):

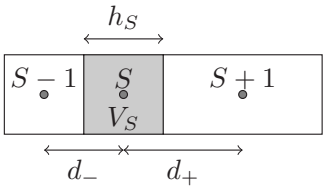

FIG. 1. 1D model system for the calculation of the exchange energy of node S with the second derivative approach [Eq. (8)]. The volume to consider is in gray.

$$e^{\mathrm{ex}} = \sum_{p,q=1}^{3} A_{pq} \frac{\partial \boldsymbol{\alpha}}{\partial r_p} \cdot \frac{\partial \boldsymbol{\alpha}}{\partial r_q}, \tag{4}$$

where A is the exchange stiffness tensor given by

$$A_{pq} = \frac{1}{4V_c} \sum_{s \in V_c} \sum_{t \in \mathcal{V}(s)} J_{st} m_s m_t \epsilon_{st} r_{st,p} r_{st,q}. \tag{5}$$

V_c is the volume of the primitive cell of the considered crystal. The sum runs on all the atoms t in the neighborhood $\mathcal{V}(s)$ of s, for each atom s in V_c. Parameter ϵ_{st} is equal to 1 or -1 depending on the relative orientation, ferromagnetic or antiferromagnetic, of the two spins s and t. We have also noted $r_{st,p}=r_{t,p}-r_{s,p}$. In the following we will only consider the case when A is diagonal, so that $A_{pq}=A_p\delta_{pq}$. In practice, given that A is real and symmetric, it can always be expressed in an appropriate set of coordinates associated with an orthonormal basis where it is diagonal.

In the continuum (micromagnetic) area, this formulation must be discretized on a mesh. A finite difference scheme has been adopted instead of finite element, partly because of the simplicity of creating a mesh but also because it makes the computation of the dipolar field by means of a fast multipole method (FMM) more straightforward (see Sec. III). Given that $|\boldsymbol{\alpha}|=1$, the micromagnetic formulation of the exchange energy in a volume V can be expressed in two equivalent ways:

$$E^{\mathrm{ex}} = \int_V \sum_{p=1}^{3} A_p \left| \frac{\partial \boldsymbol{\alpha}}{\partial r_p} \right|^2 d^3\boldsymbol{r}, \tag{6}$$

$$E^{\mathrm{ex}} = -\int_V \sum_{p=1}^{3} A_p \boldsymbol{\alpha} \cdot \frac{\partial^2 \boldsymbol{\alpha}}{\partial r_p^2} d^3\boldsymbol{r}. \tag{7}$$

Both expressions can be envisaged for the discretization. We consider for example the system of Figs. 1 and 2. We call $\mathcal{A}$ the area of the interface between the boxes and d_- (d_+) the distance between nodes S and $S-1$ ($S+1$), so the volume shared by the boxes is $V_-=\mathcal{A}d_-$ ($V_+=\mathcal{A}d_+$). h_S is the width of the box containing S and V_S is its volume. Using either second- or first-order polynomials for the interpolation, the energy associated with node S due to neighbors $S-1$ and $S+1$ can be written as

$$E_S^{\mathrm{ex}} = -2A_x V_S \boldsymbol{\alpha}_S \cdot \frac{d_+\boldsymbol{\alpha}_{S-1} + d_-\boldsymbol{\alpha}_{S+1} - (d_+ + d_-)\boldsymbol{\alpha}_S}{d_+ d_- (d_+ + d_-)} \tag{8}$$

for the second derivative expression [Eq. (7)], and

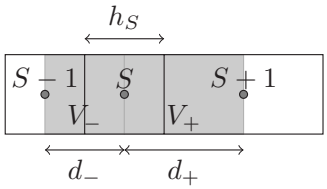

FIG. 2. 1D model system for the calculation of the exchange energy of node S with the first derivative approach [Eq. (9)]. The volumes to consider are shared by the boxes and are in gray.

$$E_S^{\mathrm{ex}} = A_x \left(\frac{V_+}{2} \left| \frac{\boldsymbol{\alpha}_{S+1} - \boldsymbol{\alpha}_S}{d_+} \right|^2 + \frac{V_-}{2} \left| \frac{\boldsymbol{\alpha}_{S-1} - \boldsymbol{\alpha}_S}{d_-} \right|^2 \right) \tag{9}$$

for the first derivative one [Eq. (6)].

In Figs. 3 and 4 we show the energy density of a domain wall on a nonuniform mesh after the first step of energy minimization in both cases. As can be seen, the stencil used in Eq. (8) introduces numerical instabilities: The energy density of large boxes in contact with small boxes is underestimated and these small boxes undergo an abnormal rise in energy. The approach of Eq. (9) has therefore been adopted. In a one-dimensional model, it consists of considering a linear variation of the angle of the magnetization between two adjacent nodes.

The transition from the micromagnetic area to the atomistic area is done with the same assumption of a linear variation of the angle of the magnetization between two adjacent nodes, one being atomic and the other one micromagnetic. For the sake of simplicity we consider the transition between a simple orthorhombic crystal of parameters a, b, and c and the continuum, as shown in Fig. 5. The axes of this lattice are aligned with the edges of the boxes to determine in a simple way the volume shared by the nodes. Exchange coupling is assumed to exist only between nearest neighbors. The transition between different levels in the continuum is also shown in Fig. 5.

In all cases, it is possible to define exchange couplings $J_{\sigma\tau}$ between nodes. If node σ is micromagnetic ($\sigma \equiv S$), effective

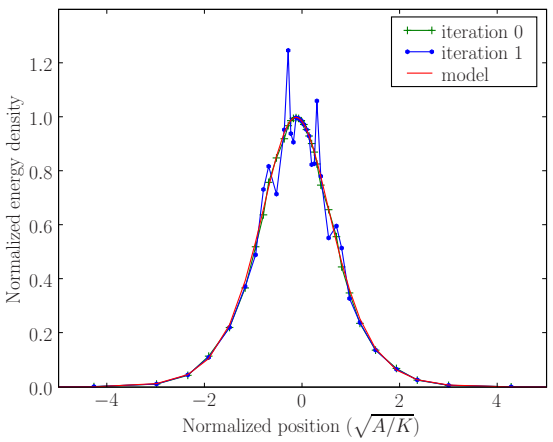

FIG. 3. (Color online) Energy density of a domain wall in a 1D system on a nonuniform mesh, initially and after one iteration of minimization. The energy is computed with the second derivative approach [Eq. (8)].

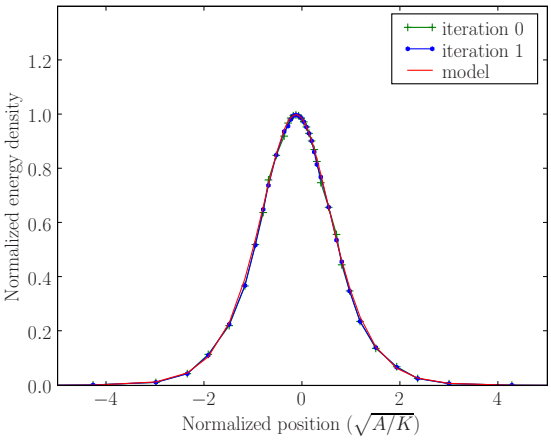

FIG. 4. (Color online) Energy density of a domain wall in a 1D system on a nonuniform mesh, initially and after one iteration of minimization. The energy is computed with the first derivative approach [Eq. (9)].

coupling constants $J_{S\tau}$ account for the variation of the magnetization between the nodes:

$$E_{S\tau}^{\mathrm{ex}} = A_x V_{S\tau} \left| \frac{\boldsymbol{\alpha}_S - \boldsymbol{\alpha}_\tau}{d_{S\tau}} \right|^2 \rightarrow J_{S\tau} = \frac{2A_x V_{S\tau}}{d_{S\tau}^2}.$$

$V_{S\tau}$ is the volume shared by nodes S and τ. Considering the coupling between the atomistic and micromagnetic regions showed in Fig. 5, it can be written $V_{St}=bcd_{St}$. Due to the separability of the exchange energy in contributions from the variation of $\boldsymbol{\alpha}$ along x, y and z [Eq. (6)], independent sets of nonoverlapping volumes can be defined for each direction. This property does not hold if the exchange stiffness tensor has off-diagonal terms.

At the boundaries of a system described within micromagnetic formalism, Brown's condition should be verified. It states that the derivative of the magnetization along the normal at the surface is zero that is in the case of Fig. 5:

$$\left. \frac{\partial \boldsymbol{\alpha}}{\partial x} \right|_{x=L} = \mathbf{0}. \tag{10}$$

To satisfy this condition we use a node outside the system, noted V in Fig. 5, in a box which has the same size as the box on the other side of the boundary. Within our approximation of exchange energy, the derivative is zero if $\boldsymbol{\alpha}_V=\boldsymbol{\alpha}_U$. This means that the energy density in the part of the system between U and V must be zero to respect Brown's condition. In practice, node V does not need to be explicitly defined.

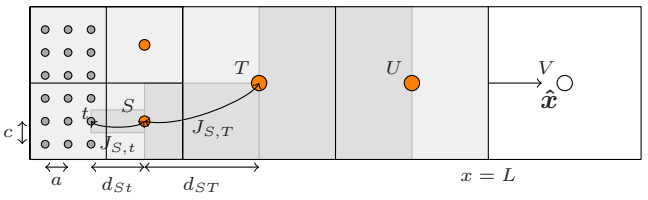

FIG. 5. (Color online) Interface between atomistic and micromagnetic areas in the case of a simple orthorhombic lattice. The boundary of the system is between nodes U and V.

B. Anisotropy energy

We consider here the case of a uniaxial anisotropy, but the same treatment can be applied to all other types of anisotropy. The magnetic anisotropy of an atomic site is

$$E_s^a = K_s[1 - (\boldsymbol{\alpha}_s \cdot \boldsymbol{u}_s)^2], \tag{11}$$

where $\boldsymbol{u}_s$ is the easy or hard axis of magnetization.

We have assumed in Sec. II A that the exchange energy density is constant between two nodes; similarly we consider that the magnetization is constant over a micromagnetic box, so that the energy in a box of volume V_S is also constant and reads

$$E_S^a = V_S K_S[1 - (\boldsymbol{\alpha}_S \cdot \boldsymbol{u}_S)^2]. \tag{12}$$

K_S is the anisotropy per unit volume and is deduced from the atomic quantities, provided that the axes $\boldsymbol{u}_s$ are the same and equal to $\boldsymbol{u}_S$ for all atoms in the box.

III. DIPOLAR TERM

A. Energy formulation

The evaluation of the dipolar energy is the most computationally demanding part of a simulation, for it is a long-range interaction. Using a direct summation in an atomistic approach leads to a computation time that scales as n_a^2, where n_a is the number of spins. As for the exchange and anisotropy energies, we start with the dipolar interaction expressed for classical atomic spins. The scalar magnetic potential created by a dipole moment $\boldsymbol{m}_s$ reads

$$\Phi^d(\boldsymbol{m}_s, \boldsymbol{r} - \boldsymbol{r}_s) = \frac{\mu_0}{4\pi} \boldsymbol{m}_s \cdot \boldsymbol{\nabla}_{\boldsymbol{r}_s} \left(\frac{1}{|\boldsymbol{r} - \boldsymbol{r}_s|} \right), \tag{13}$$

so the dipolar energy between the two moments $\boldsymbol{m}_s$ and $\boldsymbol{m}_t$ is

$$E_{st}^d = \boldsymbol{m}_t \cdot \boldsymbol{\nabla}_{\boldsymbol{r}_t} \Phi^d(\boldsymbol{m}_s, \boldsymbol{r}_t - \boldsymbol{r}_s). \tag{14}$$

Similarly, the energy of interaction between an atomic spin s and a continuous distribution of magnetization in a volume V_T, or between two continuous distributions of magnetization of volumes V_S and V_T, are

$$E_{\sigma T}^d = \int_{V_T} \boldsymbol{M}_T(\boldsymbol{r}) \cdot \boldsymbol{\nabla}_{\boldsymbol{r}} \Psi_\sigma^d d^3\boldsymbol{r}, \tag{15}$$

where Ψ_σ^d is given in the two cases ($\sigma \equiv s$ or $\sigma \equiv S$) by

$$\Psi_s^d(\boldsymbol{r}) = \Phi^d(\boldsymbol{m}_s, \boldsymbol{r} - \boldsymbol{r}_s)$$

$$\Psi_S^d(\boldsymbol{r}) = \int_{V_s} \Phi^d(\boldsymbol{M}_S(\boldsymbol{r}'), \boldsymbol{r} - \boldsymbol{r}') d^3\boldsymbol{r}'. \tag{16}$$

To be consistent with the exchange and anisotropy energies, we make the assumption that the magnetization is constant over a box. We note this constant value M_S. Ψ_S^d can be rewritten under the following form:

$$\Psi_S^d(\boldsymbol{r}) = \frac{\mu_0}{4\pi} M_S \int_{S_S} \frac{\boldsymbol{\alpha}_S \cdot d\boldsymbol{S}'}{|\boldsymbol{r} - \boldsymbol{r}'|}, \tag{17}$$

where $d\boldsymbol{S}'$ is the outward surface element.

It is also possible to rewrite the energy:

$$E^d_{\sigma T} = M_T \int_{S_T} \Psi^d_\sigma(\boldsymbol{r}) \boldsymbol{\alpha}_T \cdot d\boldsymbol{S}. \tag{18}$$

In all cases, it is possible to express the energy as

$$E^d_{\sigma\tau} = \boldsymbol{\alpha}^t_\sigma D_{\sigma\tau} \boldsymbol{\alpha}_\tau, \tag{19}$$

where the matrix elements D^{pq}_{st}, D^{pq}_{sT}, and D^{pq}_{ST} $(p,q=1,3)$ are given by

$$D^{pq}_{st} = \frac{\mu_0}{4\pi} m_s m_t \left(\frac{1}{r^3_{st}} \delta_{pq} - 3 \frac{r_{st,p} r_{st,q}}{r^5_{st}} \right),$$

$$D^{pq}_{sT} = \frac{\mu_0}{4\pi} m_s M_T \int_{S_T} \frac{r_p - r_{s,p}}{|\boldsymbol{r} - \boldsymbol{r}_s|^3} dS_q,$$

$$D^{pq}_{ST} = \frac{\mu_0}{4\pi} M_S M_T \int_{S_T} \int_{S_S} \frac{1}{|\boldsymbol{r} - \boldsymbol{r}'|} dS'_p dS_q. \tag{20}$$

Analytic expressions can be found for the two last matrix elements.[12] In these formulas, $dS_p = \boldsymbol{e}_p \cdot d\boldsymbol{S}$, where $\boldsymbol{e}_p$ is the unit vector along direction p. Two opposite surfaces with a different sign for dS_p contribute to a given direction p. In the first expression, $r_{st,p} = r_{t,p} - r_{s,p}$.

Despite the dramatic decrease in the number of variables in the system due to the multiscale approach, the direct summation of all these dipolar energy terms is in practice still too computationally demanding. In Sec. III B we present a fast summation scheme to solve this problem.

B. Fast multipole method

The FMM, as introduced by Greengard and Rokhlin[13] for coulombic interactions, is an algorithm which relies on the gathering of particles by means of multipole and local expansions to achieve an order N computation of a field or a potential.

A fundamental aspect is the ability to separate in the kernel the variables of the source (r', θ', ϕ') and those of the target (r, θ, ϕ). This is done in the case of the coulombic interaction of charged particles by the use of spherical harmonics (in the following $r > r'_s$):

$$\Phi^c(\boldsymbol{r}) = \sum_{s=1}^{n_a} \frac{1}{|\boldsymbol{r} - \boldsymbol{r}'_s|} = \sum_{l=0}^{\infty} \sum_{m=-l}^{l} M^m_l \frac{Y^m_l(\theta, \phi)}{r^{l+1}}. \tag{21}$$

Coefficients M^m_l are known as the moments of the expansion and are given by

$$M^m_l = \sum_{s=1}^{n_a} r'^l_s Y^{-m}_l(\theta'_s, \phi'_s). \tag{22}$$

Conventions for the spherical harmonics $Y^m_l(\theta, \phi)$ are those of Ref. 14. The decomposition of the dipolar kernel can be readily deduced from the previous expression:

$$\Phi^d(\boldsymbol{r}) = \frac{\mu_0}{4\pi} \sum_{s=1}^{n_a} \boldsymbol{m}_s \cdot \boldsymbol{\nabla}_{\boldsymbol{r}'_s} \left(\frac{1}{|\boldsymbol{r} - \boldsymbol{r}'_s|} \right) = \frac{\mu_0}{4\pi} \sum_{l=0}^{\infty} \sum_{m=-l}^{l} M^m_l \frac{Y^m_l(\theta, \phi)}{r^{l+1}} \tag{23}$$

with

$$M^m_l = \sum_{s=1}^{n_a} \boldsymbol{m}_s \cdot \boldsymbol{\nabla}_{\boldsymbol{r}'_s} (r'^l_s Y^{-m}_l(\theta'_s, \phi'_s)). \tag{24}$$

The method proceeds in two steps and uses a hierarchical structure of boxes to gain efficiency: First the multipole expansions are formed and they are merged upwards in the hierarchy to create the multipole expansions of larger boxes. Then these expansions are converted into local expansions:

$$\Phi^d(\boldsymbol{r}) = \frac{\mu_0}{4\pi} \sum_{l=0}^{\infty} \sum_{m=-l}^{l} L^m_l r^l Y^m_l(\theta, \phi), \tag{25}$$

which means the origin is changed from the center of source boxes to the center of target boxes. Local expansions are merged as the hierarchy is traversed downwards.

This two-step process can be used regardless of the kind of description for the sources and targets. Only the creation of the multipole expansions and the evaluation of the energy have to be adapted to each case.

The multipole expansion coefficients of the potential Ψ^d_S created by a uniform distribution of magnetization are deduced from Eqs. (17), (21), and (22):

$$M^m_l = M_S \int_{S_S} r'^l Y^{-m}_l(\theta', \phi') \boldsymbol{\alpha}_S \cdot d\boldsymbol{S}'. \tag{26}$$

They are determined using the Cartesian expression of the solid harmonics (see Appendix B).

In practice, to evaluate the energy we do not use directly expressions (14) and (18). Instead we determine a corresponding field $\boldsymbol{b}_\sigma$, which is defined as the derivative of the energy with respect to our variables $\boldsymbol{\alpha}_\sigma$. It is used to find the direction of descent in the minimization of the energy. The energy is then obtained from the expression of the field by:

$$E^d = -\frac{1}{2} \sum_\sigma \boldsymbol{\alpha}_\sigma \cdot \boldsymbol{b}_\sigma. \tag{27}$$

The field created by a node σ on a node τ is deduced from expressions (14) and (18) as

$$\boldsymbol{b}_t = -\boldsymbol{\nabla}_{\boldsymbol{\alpha}_t} E^d_{\sigma t} = -\frac{\mu_0}{4\pi} m_t \boldsymbol{\nabla}_{\boldsymbol{r}_t} \Psi^d_\sigma,$$

$$\boldsymbol{b}_T = -\boldsymbol{\nabla}_{\boldsymbol{\alpha}_T} E^d_{\sigma T} = -\frac{\mu_0}{4\pi} M_T \int_{S_T} \Psi^d_\sigma(\boldsymbol{r}) d\boldsymbol{S}. \tag{28}$$

It is worth noting that by rewriting this latest equation we obtain that the field on a micromagnetic node is the average of the field over the box containing this node:

$$\boldsymbol{b}_T = -\frac{\mu_0}{4\pi} M_T \int_{V_T} \boldsymbol{\nabla}_{\boldsymbol{r}} \Psi^d_\sigma d^3\boldsymbol{r}. \tag{29}$$

The conversion of a multipole expansion into a local expansion imposes that interacting boxes are far enough from each other.[14] When this is not the case, a direct summation has to be done, using the set of equations in Eq. (20). It is worth mentioning that a box can be surrounded by boxes at different levels, so this summation may extend beyond nearest neighbors. Particular care has to be taken for neighbor boxes that contain atomic and micromagnetic nodes.

C. Transition between atomistic and micromagnetic description

The computation of the dipolar interaction between near atomic and micromagnetic nodes may lead to several difficulties, namely (i) the energy of interaction between the charged surface and the atomic spin is not well defined numerically if the spin is on the surface and (ii) summing over a lattice to compute the field implicitly takes into account the geometry of the lattice, which does not occur for an atomic site near a micromagnetic region.

This latest remark also applies to the computation of the field in micromagnetic regions. Including the effects of the lattice can be done using Lorentz's approach which consists of writing the local field as follows:[3]

$$\boldsymbol{b}_{T,\mathrm{loc}} = \boldsymbol{b}_T + D_T \boldsymbol{\alpha}_T + \Lambda_T \boldsymbol{\alpha}_T, \tag{30}$$

where D_T is a matrix accounting for the magnetic charges at the surface of a cavity around T, Λ_T is a traceless matrix that is determined by a summation on the lattice sites inside the cavity, and $\boldsymbol{b}_T$ is the field created by charges beyond the cavity. The cavity must be sufficiently large to correctly take into account the geometry effects included in Λ_T, but $\boldsymbol{\alpha}$ should have at most linear variations in it, which is in practice always verified in micromagnetic regions.

The effect of the geometry of the lattice on the local field is highlighted in Fig. 6, where a distortion of the lattice from cubic to tetragonal is envisaged. We take $\mu_0=1$ and keep the value of the magnetization M equal to 1, so that a typical demagnetizing field is also 1. It can be clearly seen that even with moderate distortions, the contribution of Λ_T to the dipolar field cannot be neglected. However, a good precision on this term can be reached by summing only on a few atomic layers (Fig. 7).

The last two terms of Eq. (30) are systematically added to get the local field in micromagnetic boxes. To compute the field on an atomic site near micromagnetic boxes, a summation on virtual lattice sites inside these boxes is used to determine a dipolar interaction matrix between the atomic spin and the macrospin. This enables one to correctly take into account the lattice geometry and to remove the problem noted in remark (i).

The largest error on the field comes from the position of the interface between the atomistic and micromagnetic regions imposed by the mesh. It may differ from the position ensuring a correct value of the magnetization around the interface. The value of the field in the middle of an atomic cavity with a large mismatch between the correct and actual position of the interface is shown in Fig. 8. This effect imposes a minimum number of atomic layers around the atomic sites to reduce the error. The summation on virtual lattice sites that extends through near micromagnetic neighbors helps to minimize the error and may be extended to further neighbors if a higher precision is required.

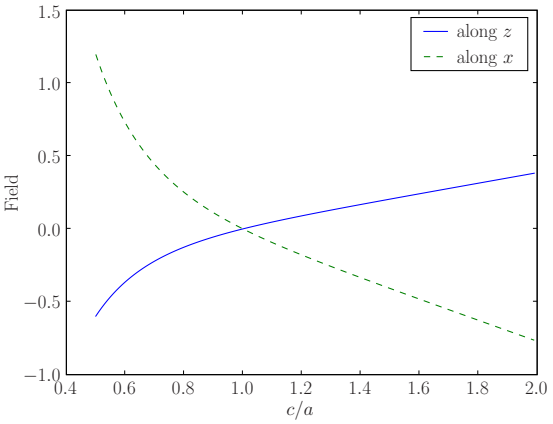

FIG. 6. (Color online) Dipolar field due to the lattice effects for different tetragonal distortions c/a. The magnetization is along x or z and the field is computed in the direction of the magnetization. $M=1$ and $\mu_0=1$, so a typical demagnetizing field is around 1. The shape effects due the sample used for the summation are corrected and do not contribute to the field.

IV. NUMERICAL CONSIDERATIONS

The properties of the mesh used to compute the energy have not been specified so far. At each step, boxes can be divided, resolved at the atomic scale or gathered according to the spatial variations of the magnetization. The presence of structural inhomogeneities can also force the description at the atomic scale. The criteria used to remesh a given system are derived in this section. For convenience, they are based on the spatial variation of our variables $\boldsymbol{\alpha}_\sigma$ but should ensure a good evaluation of the energy. To explain the procedure, we use in the following a unidimensional system.

We first consider the approximate value of the uniaxial anisotropy energy of a box in such a unidimensional system.

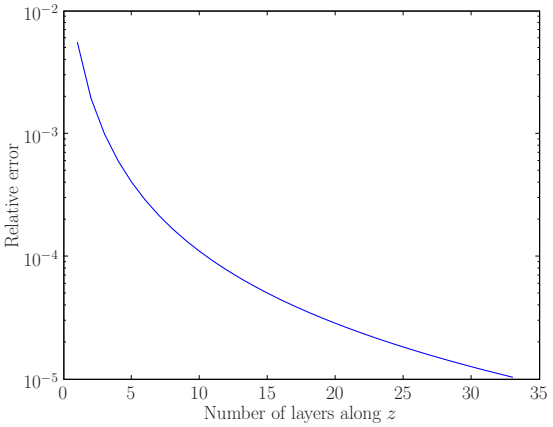

FIG. 7. (Color online) Relative error on the field due to the lattice effects as a function of the number of layers taken into account to compute this field. The tetragonal distortion is $c/a=3$, but the global shape of the system is cubic (no shape effect).

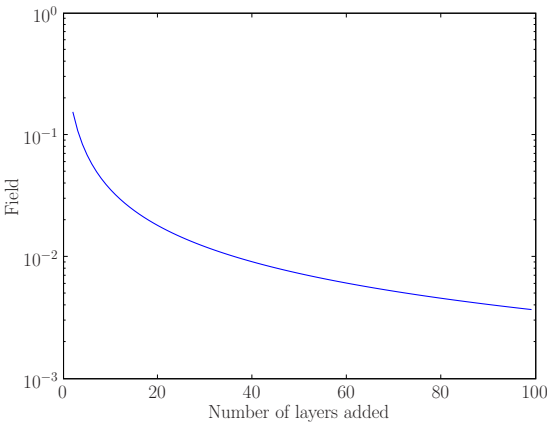

FIG. 8. (Color online) Influence of the mismatch between the correct position of the interface between atomic/micromagnetic regions and its actual position. $M=1$ and $\mu_0=1$, so a typical demagnetizing field is around 1. A high modification of the shape effect is envisaged here for a simple cubic lattice: The four surfaces with normals along $\pm\hat{\boldsymbol{x}}$ and $\pm\hat{\boldsymbol{y}}$ are shifted toward the center of the box of $a/2$ (with $a=1$), and the two surfaces along $\pm\hat{\boldsymbol{z}}$ are shifted away from the center of the same quantity. See Fig. 9 for the geometry of the system.

Energies are normalized by $\sqrt{AK}$ and distances by $\delta=\sqrt{A/K}$. h is the length of this box in units of δ, so the energy reads at order 2:

$$\begin{aligned} E_h^a &= -\int_{-h/2}^{h/2} (\boldsymbol{\alpha}\cdot\boldsymbol{u})^2 dx \\ &= -\int_{-h/2}^{h/2} \left[(\boldsymbol{\alpha}_0\cdot\boldsymbol{u})^2 + \frac{1}{2}x^2 \frac{d^2}{dx^2}(\boldsymbol{\alpha}\cdot\boldsymbol{u})^2 \bigg|_0 \right] dx \\ &= -h(\boldsymbol{\alpha}_0\cdot\boldsymbol{u})^2 - \frac{h^3}{24}\frac{d^2}{dx^2}(\boldsymbol{\alpha}\cdot\boldsymbol{u})^2 \bigg|_0 . \end{aligned} \tag{31}$$

The quantities tagged with zeros are taken in the middle of the box. Our multiscale approach neglects the term at order 2 in this expression, so the criteria to remesh should be defined to minimize its contribution to the energy. Expanding it leads to

$$\frac{d^2}{dx^2}(\boldsymbol{\alpha}\cdot\boldsymbol{u})^2 \bigg|_0 = 2\left[(\boldsymbol{\alpha}_0\cdot\boldsymbol{u}) \left(\frac{d^2\boldsymbol{\alpha}}{dx^2}\bigg|_0 \cdot\boldsymbol{u} \right) + \left(\frac{d\boldsymbol{\alpha}}{dx}\bigg|_0 \cdot\boldsymbol{u} \right)^2 \right]. \tag{32}$$

Similarly the exchange energy between two nodes separated of h can be written at order 2 as

$$E_h^{\mathrm{ex}} = h\left(\frac{d\boldsymbol{\alpha}}{dx}\bigg|_0 \right)^2 + \frac{h^3}{24}\frac{d^2}{dx^2}\left(\frac{d\boldsymbol{\alpha}}{dx} \right)^2 \bigg|_0 . \tag{33}$$

Here the quantities subscripted by 0 are taken in the middle of the two nodes. However the first derivative is not known exactly and it should be replaced by its approximation at order 2:

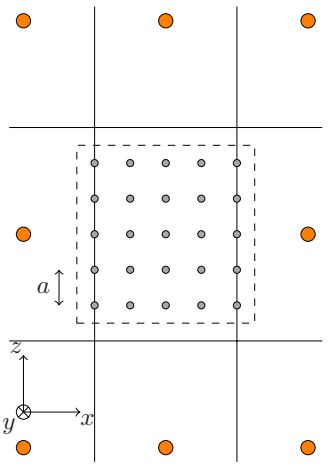

FIG. 9. (Color online) System used to study the influence of the position of the interface between atomic and micromagnetic regions on the field on an atomic site. Here the field is computed on the atomic site at the center of the box. The ideal position of the interface is shown in dashed lines. In the figure, two layers of atoms have been added around the atom at the center.

$$\left(\frac{d\boldsymbol{\alpha}}{dx}\bigg|_0 \right)^2 = \left(\frac{\boldsymbol{\alpha}_+ - \boldsymbol{\alpha}_-}{h} \right)^2 - \frac{h^2}{12}\frac{d\boldsymbol{\alpha}}{dx}\bigg|_0 \cdot \frac{d^3\boldsymbol{\alpha}}{dx^3}\bigg|_0 , \tag{34}$$

where $\boldsymbol{\alpha}_+$ and $\boldsymbol{\alpha}_-$ are the values of $\boldsymbol{\alpha}$ at the two nodes. Therefore the second-order term in the energy is simply

$$\frac{h^3}{24}\frac{d^2}{dx^2}\left(\frac{d\boldsymbol{\alpha}}{dx} \right)^2 \bigg|_0 - \frac{h^3}{12}\frac{d\boldsymbol{\alpha}}{dx}\bigg|_0 \cdot \frac{d^3\boldsymbol{\alpha}}{dx^3}\bigg|_0 = \frac{h^3}{12}\left(\frac{d^2\boldsymbol{\alpha}}{dx^2}\bigg|_0 \right)^2 . \tag{35}$$

To refine a mesh, first and second derivatives of $\boldsymbol{\alpha}$ should therefore be taken into account: If in a box, the criteria

$$\begin{cases} h^2 \left| \dfrac{d\boldsymbol{\alpha}}{dx} \right|^2 \le \epsilon \\ h^2 \left| \dfrac{d^2\boldsymbol{\alpha}}{dx^2} \right| \le \epsilon \end{cases} \tag{36}$$

are not met, then we either divide the box or resolve it at atomic scale if it does not contain enough atoms. In our simulations, ϵ is taken equal to 0.04 and called ϵ_d. A different value, $\epsilon_g=0.01$, is considered to decide when boxes should be gathered. This set of two criteria avoids oscillations of the mesh between two configurations.

It is worth noting that it can be advantageous to adopt less stringent conditions at the beginning of the minimization: The obtained coarsened mesh is useful to propagate information rapidly from one point of the system to another, thus alleviating a drawback of nonpreconditioned or diagonally preconditioned conjugate gradient methods. A typical case where this strategy proves useful is the formation of a large domain wall of width δ in a unidimensional system containing initially an abrupt change of magnetization: For example if δ is around 1000 interatomic distances, the convergence is obtained after 380 iterations without any change of criteria, whereas with $\epsilon_d=0.26$ and $\epsilon_g=0.06$ at the beginning of the

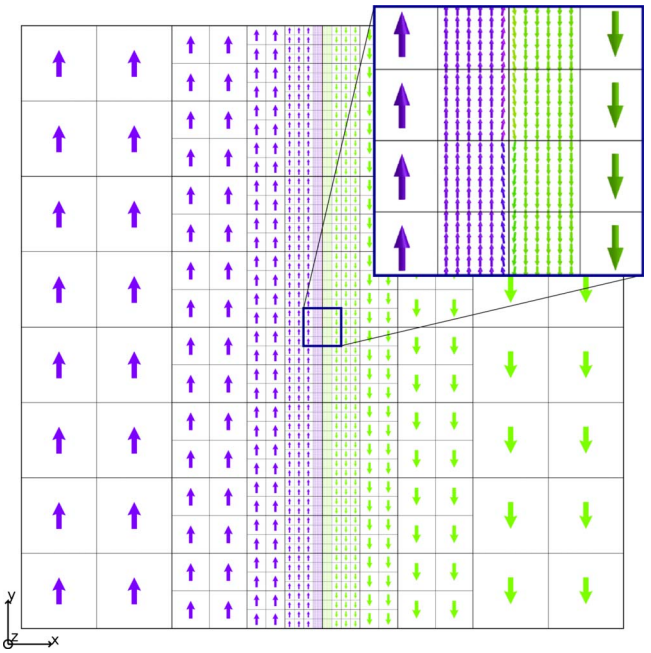

FIG. 10. (Color online) Initial configuration to create a vortex: The system contains two domains separated by an abrupt domain wall; at the center of the system the spins are slightly tilted to be compatible with the formation of a vortex (inset).

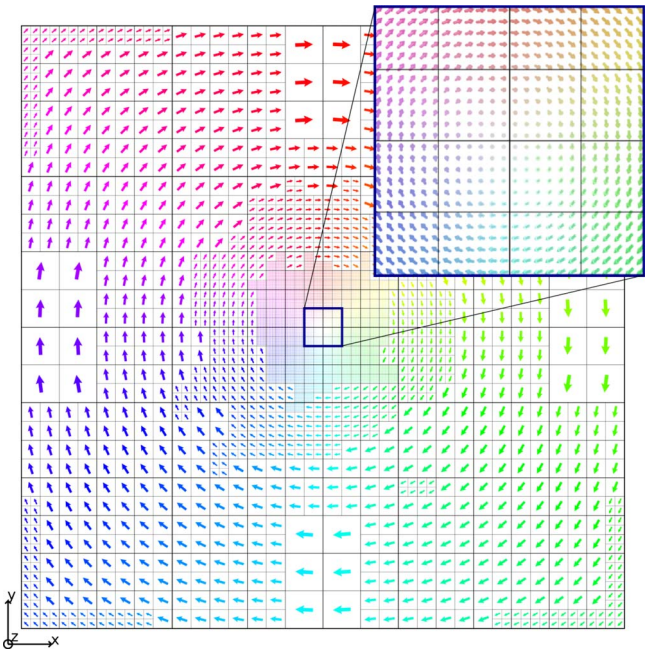

FIG. 11. (Color online) Configuration of the vortex after an energy minimization. The inset shows the magnetic structure near the core of the vortex. Asymmetries in the mesh are due to the fact that criteria to divide or gather boxes may not be met at the same iteration in symmetric parts of the system, because of numerical precision. Moreover these asymmetries may be persistent given the different values considered for ϵ_d and ϵ_g that make the gathering of boxes more difficult than their division.

minimization the convergence is reached after only 220 iterations. The use of a fully atomistic description results in a convergence after 2190 iterations.

In addition to these criteria on the spatial variation of magnetization, some geometrical criteria should also be met: We impose that two adjacent boxes do not differ by more than one level and try to minimize the area of interfaces between boxes from different levels.

V. APPLICATIONS

A. Vortex in a thin square element

In this section the multiscale method is applied to the study of a vortex in a thin square element. A multiscale simulation is well adapted to such a system because the magnetization rotates rapidly near the center of the vortex, while the rest of the system exhibits low variations of magnetization. The use of the Heisenberg model near the center of the vortex removes the singularity of the energy density observed in micromagnetics.

To illustrate the need for an adaptive mesh refinement, we start with the configuration shown in Fig. 10. A domain wall is placed in the middle of the system, with a small misorientation of the spins at the center compatible with the formation of a vortex. The final configuration after a minimization of the energy is shown in Fig. 11. The exchange coupling between first neighbors in a simple cubic lattice is $J=4$ meV$/\mu_b^2$. The atomic moments are $m=4\mu_b$ and the anisotropy is set to zero. These values are typical parameters for magnetically soft materials, such as Permalloy $Ni_{80}Fe_{20}$.

The dimensions of the system are 140 nm$\times$140 nm $\times$3.5 nm and the lattice parameter is $a=0.35$ nm, so the total number of atoms accounted for is 1.6 million. With such a number of atoms, a parallel implementation of the atomistic code that also computes the dipolar field with the FMM has been used to provide a reference calculation. A comparison with a micromagnetic approach based on a uniform mesh of 65536 nodes has also been performed. In Fig. 12 we have plotted the out-of-plane component of the magnetization (along z) on a line crossing the center of the vortex. It can be seen that the three approaches agree very well.

The good agreement with the micromagnetic approach is ensured by using a mesh step of 1.1 nm$\times$1.1 nm

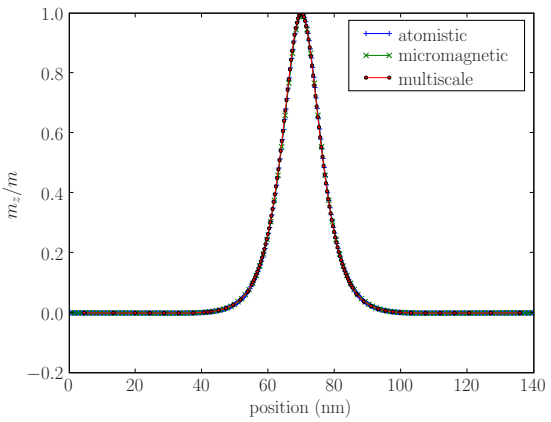

FIG. 12. (Color online) Component of the magnetization along z on a line crossing the vortex core for the different approaches: fully atomistic, micromagnetic, and multiscale.

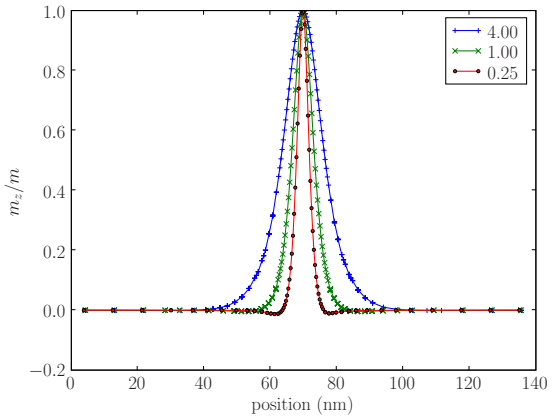

FIG. 13. (Color online) Component of the magnetization along z on a line crossing the vortex core for a multiscale simulation. Different values of exchange couplings J are envisaged (in meV/μ_b^2). Negative values of m_z can be observed near the vortex core for $J=0.25$ meV/μ_b^2 and they are ascribed to the dipolar field created by the magnetization in the core (see Refs. 15 and 16).

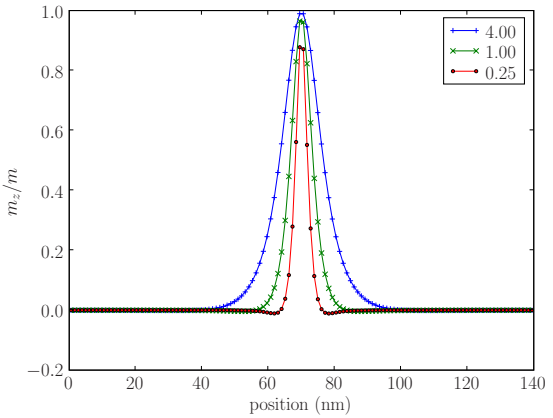

FIG. 14. (Color online) Component of the magnetization along z on a line crossing the vortex core for a micromagnetic simulation. Different values of exchange couplings J are envisaged (in meV/μ_b^2). Note the poor precision on m_z at the core of the vortex when J is 0.25 meV/μ_b^2, compared to the multiscale simulation in Fig. 13.

$\times 0.9$ nm, which is below the exchange length $\sqrt{A/(1/2\mu_0 M_s^2)}=5.8$ nm. Decreasing the exchange coupling J and thus the exchange stiffness constant A triggers a decrease in the exchange length, which can lead to significant errors in the evaluation of the magnetization near the vortex core in the micromagnetic approach. This is emphasized in Figs. 13 and 14, where the same level for the fine mesh has been kept while decreasing J. To accelerate the convergence, the initial configuration consists of four closure domains with the magnetization along x or y, with a sharp transition between them. The number of variables is roughly constant in the multiscale simulation and is around 20000. It remains far below the number of variables needed for the micromagnetic simulation on a uniform mesh, while keeping a good precision on the result.

B. Microtwins and domain walls in FePt thin films

Our multiscale method is applied here to the study of the interaction of domain walls with structural defects in thin layers of FePt. It has been shown experimentally that in thin films of $L1_0$ FePt deposited on a buffer layer of Pt, structural defects called microtwins play a major role in the propagation behavior of domain walls.[17] In such alloys exhibiting very high magnetocrystalline anisotropy of the order of 1 meV per Fe atom, domain walls are strongly pinned to these defects.[2]

The use of the multiscale approach is particularly interesting here due to its ability to precisely describe the structural defects at the atomic scale. Microtwins are formed by the accumulation of stacking faults along the {111} planes, so the core of these defects can be seen as a tilted $L1_0$ lattice. A model proposed by Néel[18] is used in both atomistic and multiscale methods to compute the anisotropy of the system. This enables one to systematically take into account the contribution of the local atomic configuration to the magnetic anisotropy. Following *ab initio* calculations,[19] a smaller exchange constant ($J=0.15$ meV/μ_b^2) is taken along the c axis of the $L1_0$ material than along the a axis ($J=3.45$ meV/μ_b^2). The coupling is in all cases between nearest neighbors. We assume that Pt atoms have no magnetic moment and only contribute to the anisotropy of Fe atoms. The moment of Fe atoms is $3.06\mu_b$. The micromagnetic simulation of the system will not be envisaged here, because it would require to deal with a nondiagonal exchange stiffness tensor in the microtwin and related boundary conditions between the microtwin and the rest of the system.

A configuration with the domain wall out of the microtwin is shown in Fig. 15. The configuration with the pinned domain wall can be seen in Fig. 16. The microtwin is always described at the atomic scale. The system is periodic along direction y and contains 40 Fe atomic planes along z.

Once the domain wall is pinned to the microtwin, the depinning field depends on the direction of the field, as was shown in Ref. 2. This is highlighted in Table I, where the

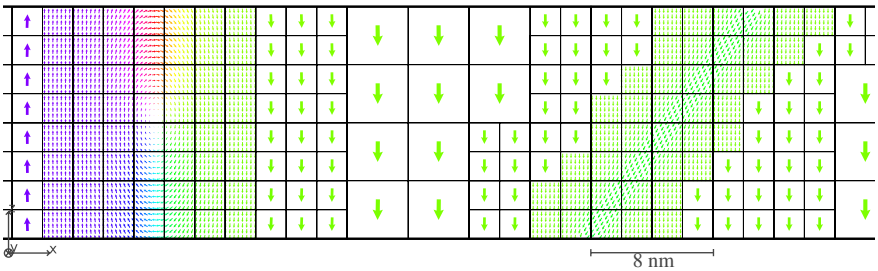

FIG. 15. (Color online) Domain wall (on the left) out of the microtwin (on the right). The domain wall contains a Bloch core with two Néel caps due to the dipolar interaction. The microtwin is 6 atomic planes wide and the system contains 40 Fe atomic planes along z.

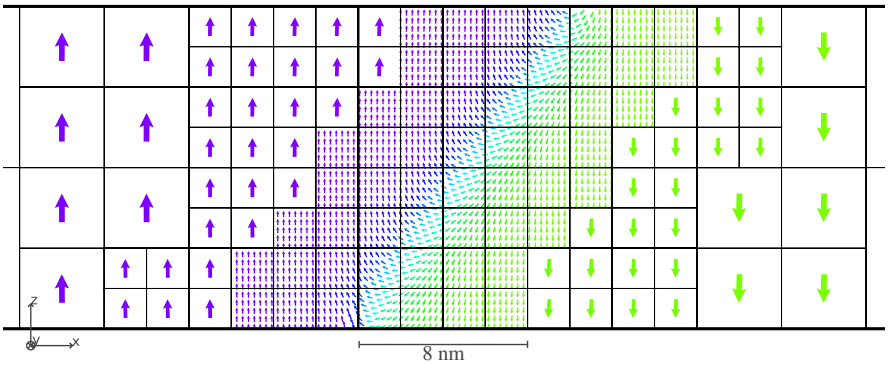

FIG. 16. (Color online) Domain wall pinned to the microtwin. The microtwin is 6 atomic planes wide and the system contains 40 Fe atomic planes along z.

depinning field is given as a function of the width of the microtwin. It can be seen that the multiscale method agrees very well with the atomistic approach.

VI. CONCLUSION

We have presented a multiscale method for the simulation of magnetic systems that seamlessly couples classical Heisenberg model to micromagnetics. A multiresolution adaptive finite difference mesh is used to compute the energy and the local field. The hierarchical structure of the mesh makes possible the evaluation of the dipolar term with an order N fast summation scheme.

This method has been used to determine the magnetic configuration of a thin square element where the initial state consists of an abrupt domain wall in the middle of the system. The resulting vortex is well described by the method and compared to both fully atomistic and micromagnetic approaches. Another example of application is the interaction between a domain wall and a microtwin in a thin layer of FePt. The depinning fields are found in very good agreement with fully atomistic computations.

Advantages in terms of number of variables and precision are significant and make such a multiscale approach attractive for large magnetic systems where some specific regions should be described at atomic scale, either because of steep variations of magnetization or because of the presence of structural defects.

TABLE I. Depinning fields on the left (b_l) or on the right (b_r) for a domain wall initially propagating from the left to the right, in the atomistic and multiscale approaches. Uncertainty on the values is 5 mT. The width of the microtwin w is in number of atomic planes. The layer contains 40 Fe atomic planes.

	Atomistic		Multiscale	
w (at. planes)	b_l (T)	b_r (T)	b_l (T)	b_r (T)
3	−1.315	1.645	−1.315	1.645
6	−2.305	2.835	−2.305	2.835
9	−2.785	3.495	−2.795	3.505
12	−3.015	3.595	−3.025	3.615

APPENDIX A: ATOMISTIC AND MICROMAGNETIC APPROACHES FOR EXCHANGE ENERGY

We derive here a general formula that gives the exchange energy in the micromagnetic approach using the Heisenberg model. A similar treatment has been applied for some common lattices in ferromagnets in Ref. 20.

Following Eq. (3), the exchange energy density within the Heisenberg model can be written as

$$e^{\mathrm{ex}} = -\frac{1}{2V_c}\sum_{s\in V_c}\sum_{t\in\mathcal{V}(s)} J_{st} m_s m_t \boldsymbol{\alpha}_s \cdot \boldsymbol{\alpha}_t. \tag{A1}$$

The micromagnetic approach states that there is a normalized vector field $\boldsymbol{\alpha}(\boldsymbol{r})$ defined in every part of the system. To treat ferromagnets, locally collinear antiferromagnets or ferrimagnets, every atomistic variable $\boldsymbol{\alpha}_s$ must be equal or opposed to the value of this vector field at its position: $\boldsymbol{\alpha}(\boldsymbol{r}_s) = \epsilon_s \boldsymbol{\alpha}_s$, with $\epsilon_s = \pm 1$. We note $\epsilon_{st} = \epsilon_s \epsilon_t$, so that the energy density due to the coupling between spins s and t reads

$$\begin{aligned} e_{st}^{\mathrm{ex}} &= -\frac{1}{2V_c} J_{st} m_s m_t \epsilon_{st} \boldsymbol{\alpha}(\boldsymbol{r}_s) \cdot \boldsymbol{\alpha}(\boldsymbol{r}_t) \\ &= -\frac{1}{2V_c} J_{st} m_s m_t \epsilon_{st} \left[1 - \frac{(\boldsymbol{\alpha}(\boldsymbol{r}_t) - \boldsymbol{\alpha}(\boldsymbol{r}_s))^2}{2} \right]. \end{aligned} \tag{A2}$$

To be consistent with the micromagnetic formulation of exchange energy, the energy density must be zero if $\boldsymbol{\alpha}(\boldsymbol{r})$ is constant. Therefore we drop the constant term in the previous equation. Using a first-order expansion of this field, we write that

$$\boldsymbol{\alpha}(\boldsymbol{r}_t) \approx \boldsymbol{\alpha}(\boldsymbol{r}_s) + \sum_{p=1}^{3} r_{st,p} \left. \frac{\partial \boldsymbol{\alpha}}{\partial r_p} \right|_{\boldsymbol{r}=\boldsymbol{r}_s}, \tag{A3}$$

so that the exchange energy density is

$$e_{st}^{\mathrm{ex}} = \frac{1}{4V_c} J_{st} m_s m_t \epsilon_{st} \sum_{p,q=1}^{3} r_{st,p} r_{st,q} \frac{\partial \boldsymbol{\alpha}}{\partial r_p} \cdot \frac{\partial \boldsymbol{\alpha}}{\partial r_q}. \tag{A4}$$

The total energy density and the exchange stiffness tensor are then given by Eqs. (4) and (5).

APPENDIX B: MULTIPOLE EXPANSION FOR A MACROSPIN

To evaluate the multipole expansion associated with a macrospin, or to average the field on a box, it is necessary to compute the following integral:

$$\int_S r^l Y_l^{-m}(\theta,\phi)d\boldsymbol{S}, \tag{B1}$$

where the origin is at the center of the box and the integral is evaluated over its surface. In the following we use the convention of Ref. 14 for the spherical harmonics.

A simple approach to compute this integral consists of rewriting solid harmonics $r^l Y_l^m(\theta,\phi)$, which are homogeneous polynomials, under the form

$$r^l Y_l^m(\theta,\phi) = \sum_{u=0}^{l}\sum_{v=0}^{u} C_{l,m}^{u,v} x^{l-u} y^{u-v} z^v. \tag{B2}$$

Such a decomposition has been given by Caola (Ref. 21). We give here recurrence relations to determine the coefficients $C_{l,m}^{u,v}$. Starting with the expression

$$r^l Y_l^l(\theta,\phi) = \frac{\sqrt{(2l)!}(-1)^l}{2^l l!}(x+iy)^l, \tag{B3}$$

we use the following relation:

$$Y_{l+1}^l(\theta,\phi) = \sqrt{2l+1}\,\cos\,\theta Y_l^l(\theta,\phi) \tag{B4}$$

and obtain

$$r^{l+1} Y_{l+1}^l(\theta,\phi) = \frac{\sqrt{(2l+1)!}(-1)^l}{2^l l!}(x+iy)^l z. \tag{B5}$$

Other coefficients are determined using the following recurrence relation:[22]

$$B_{l+1}^m Y_{l+1}^m(\theta,\phi) - (2l+1)Y_1^0(\theta,\phi)Y_l^m(\theta,\phi) + B_l^m Y_{l-1}^m(\theta,\phi) = 0, \tag{B6}$$

with

$$B_l^m = \sqrt{(l+m)(l-m)}. \tag{B7}$$

We obtain

$$r^{l+1} Y_{l+1}^m(\theta,\phi) = \frac{2l+1}{B_{l+1}^m} z r^l Y_l^m(\theta,\phi) - \frac{B_l^m}{B_{l+1}^m}(x^2+y^2+z^2) r^{l-1} Y_{l-1}^m(\theta,\phi), \tag{B8}$$

so the relation between coefficients reads

$$C_{l+1,m}^{u,v} = \frac{2l+1}{B_{l+1}^m} C_{l,m}^{u-1,v-1} - \frac{B_l^m}{B_{l+1}^m}(C_{l-1,m}^{u,v} + C_{l-1,m}^{u-2,v} + C_{l-1,m}^{u-2,v-2}). \tag{B9}$$

*Corresponding author. Frederic.Lancon@cea.fr

[1] H. Kronmüller and M. Bachmann, Physica B (Amsterdam) **306**, 96 (2001).
[2] T. Jourdan, F. Lançon, and A. Marty, Phys. Rev. B **75**, 094422 (2007).
[3] W. F. Brown, *Micromagnetics* (Interscience, New York, 1963).
[4] C. García-Cervera and A. Roma, IEEE Trans. Magn. **42**, 1648 (2006).
[5] R. Hertel and H. Kronmüller, IEEE Trans. Magn. **34**, 3922 (1998).
[6] F. Garcia-Sanchez, O. Chubykalo-Fesenko, O. Mryasov, R. W. Chantrell, and K. Y. Guslienko, Appl. Phys. Lett. **87**, 122501 (2005).
[7] V. V. Dobrovitski, M. I. Katsnelson, and B. N. Harmon, Phys. Rev. Lett. **90**, 067201 (2003).
[8] G. Grinstein and R. H. Koch, Phys. Rev. Lett. **90**, 207201 (2003).
[9] M. Kirschner, T. Schrefl, F. Dorfbauer, G. Hrkac, D. Suess, and J. Fidler, J. Appl. Phys. **97**, 10E301 (2005).
[10] V. B. Shenoy, R. Miller, E. b. Tadmor, D. Rodney, R. Phillips, and M. Ortiz, J. Mech. Phys. Solids **47**, 611 (1999).
[11] S. W. Sloan, Comput. Struct. **47**, 441 (1993).
[12] M. Maicas and E. Lopez, IEEE Trans. Magn. **34**, 601 (1998).
[13] L. Greengard and V. Rokhlin, J. Comput. Phys. **73**, 325 (1987).
[14] L. Greengard, *The Rapid Evaluation of Potential Fields in Particle Systems* (MIT, Cambridge, MA, 1988).
[15] J. K. Ha, R. Hertel, and J. Kirschner, Phys. Rev. B **67**, 224432 (2003).
[16] J. Raabe, R. Pulwey, R. Sattler, T. Schweinbock, J. Zweck, and D. Weiss, J. Appl. Phys. **88**, 4437 (2000).
[17] J. P. Attané, D. Ravelosona, A. Marty, Y. Samson, and C. Chappert, Phys. Rev. Lett. **96**, 147204 (2006).
[18] L. Néel, J. Phys. Radium **15**, 225 (1954).
[19] O. N. Mryasov, J. Magn. Magn. Mater. **272-276**, 800 (2004).
[20] C. Kittel, Rev. Mod. Phys. **21**, 541 (1949).
[21] M. J. Caola, J. Phys. A **11**, L23 (1978).
[22] P. M. Morse and H. Feshback, *Methods of Theoretical Physics* (McGraw-Hill, New York, 1953), Vol. 2, Chap. 10, p. 1326.